JOURNAL OF CATALYSIS 118, 227–237 (1989)

Reversibility of Strong Metal–Support Interactions on Rh/TiO_2

EHRICH J. BRAUNSCHWEIG,* A. DAVID LOGAN,* ABHAYA K. DATYE,* AND DAVID J. SMITH†

*Department of Chemical and Nuclear Engineering, University of New Mexico, Albuquerque, New Mexico 87131, and †Center for Solid State Science and Department of Physics, Arizona State University, Tempe, Arizona 85287

Received November 18, 1988; revised February 15, 1989

Hydrogenolysis of *n*-butane and CO hydrogenation were used to study the reversibility of the SMSI state in Rh supported on model nonporous TiO_2 spheres. High-temperature reduction (HTR) caused a three-order-of-magnitude drop in hydrogenolysis activity and led to increased selectivity toward ethane. Oxidation at 573 K was sufficient to restore the hydrogenolysis activity in these catalysts. Variations in hydrogenolysis selectivity on Rh/TiO_2 were similar to those on Rh/SiO_2 subjected to comparable treatments. This suggests that site blocking by TiO_x may be primarily responsible for the suppressed hydrogenolysis activity on Rh/TiO_2. CO hydrogenation activity, on the other hand, was only marginally affected by the onset of SMSI and either increased or decreased after HTR depending on the prior treatment of the catalyst. High-resolution transmission electron microscopy showed the presence of 2- to 4-Å amorphous overlayers on both the Rh and the support after high-temperature reduction. The thickness of these overlayers was nonuniform and oxidation followed by low-temperature reduction led to partial removal of the overlayers and a roughening of the Rh metal surfaces.

INTRODUCTION

A strong metal–support interaction (SMSI) on titania supports reported by Tauster *et al.* (*1*) has led to considerable research in understanding the origins of such behavior. The interest in titania supports is heightened by their unique ability to enhance the reactivity of the metal in hydrogenation of CO (*2*) or molecules that have CO functional groups (*3*), while suppressing hydrogenolysis of hydrocarbons such as ethane (*4*) or *n*-butane (*5*). The SMSI effect appears to be prevalent on both small and large metal particles, leading to the currently accepted mechanism involving decoration and local electronic perturbation (*6–8*). It was originally reported that the H_2 uptake on Pt could be restored after oxidation at 673 K (*1*). Subsequent studies have found that the adsorptive properties of the metal could be partially restored even by oxygen exposure at room temperature (*9*) or by exposure to steam at 525 K (*10*). Since the activity in hydrogenolysis reactions is affected strongly by the onset of SMSI, reactivity is a better probe than chemisorption for monitoring the reversal of SMSI. The data of Foger (*5*) show that the activity of highly dispersed Ir catalysts subjected to SMSI is restored by oxygen treatment at 470 K. On the other hand, Ir catalysts having a mean diameter of 3.5 nm had to be oxidized at 673 K to restore catalytic behavior, resulting in an irreversible change to the catalyst.

A survey of recent literature shows that while the reactivity changes after onset of the SMSI state are well documented, the reversibility of catalytic behavior has not been addressed (*2–4, 7–9, 11–15*). It is important to determine the correlation between suppression in chemisorptive uptake of H_2 and altered catalytic reactivity since TiO_2 supports have been shown to alter catalytic behavior of the metal even prior to high-temperature reduction (HTR) (*16*). Quantifying the reversibility of SMSI is important for a better understanding of the mechanisms underlying this effect.

0021-9517/89 $3.00

To quantify the reversibility of the SMSI phenomenon, we have studied the catalytic behavior of a Rh/TiO_2 catalyst that was repeatedly cycled between the low-temperature reduction (LTR) and HTR states. The activity of this catalyst for hydrogenolysis of *n*-butane and CO hydrogenation was monitored after each pretreatment. The support consisted of spherical TiO_2 single-crystal particles of the anatase and rutile phases. We have previously shown that such model supports make it possible to study surface structure and reactivity of the same catalyst (*17*). We report here a correlation between the activity and chemisorption behavior of these catalysts and the morphology of the metal particles on the atomic scale as studied in a high-resolution transmission electron microscope. The reactivity behavior of the Rh/TiO_2 catalyst is compared with that of a similar Rh/SiO_2 catalyst cycled under the same conditions to contrast SMSI behavior with phenomena induced in Rh by oxidation–reduction cycling alone.

EXPERIMENTAL

Nonporous, crystalline titania powders were synthesized in a thermal plasma yielding spherical, crystalline particles. The synthesis of these powders is based on a technique pioneered by Uyeda and co-workers (*18, 19*) and can be applied to synthesis of a variety of oxide powders whose primary particles are nonporous, single crystals of near-spherical shape. A low-magnification electron micrograph of the titania powder is shown in Fig. 1, where the particles range in diameter from 10 to 250 nm. Both anatase and rutile crystals were present in the powder and the distribution of phases was approximately 70 : 30 anatase : rutile as determined by XRD. The powder surface area was 10–15 m^2/g which confirmed the nonporous nature of the particles.

The model catalysts were made by nonaqueous impregnation of rhodium (III) 2,4-pentanedionate ($Rh(acac)_3$). Initial reduction was performed in 20 sccm of hydrogen while the temperature was raised from 300 to 423 K, held for 5 h (to prevent sublimation of the metal precursor before decomposition), and then raised to 473 K and held 4 h. High-temperature reduction was done in hydrogen at 773 K for 4 h, and the oxidation treatment was done using 10% oxygen in helium at the treatment temperature for 4 h. Hydrogen chemisorption was performed in an all-glass, static volumetric apparatus pumped with a LN_2 baffled diffusion pump. The base pressure was 1×10^{-7} Torr (1 Torr = 133 Pa). Gas pressure was measured by a Baratron capacitance manometer. Reactivity studies were carried out in a quartz U-tube microreactor using hydrogen, helium, and oxygen (UHP grade, Big Three Industries), and research-purity *n*-butane and carbon monoxide (Matheson). Flow rates were measured using a TYLAN mass flow controller. Reaction products were analyzed by a Varian 3400 GC, and the total conversion was kept below 10%. At these low conversions, there was no influence on selectivity in *n*-butane hydrogenolysis. The reactor pressure was kept at 118 kPa absolute pressure and the temperature was controlled by an Omega temperature programmer. The reactants were fed into the microreactor in a molar ratio of 20 : 1 H_2 : *n*-butane or 3 : 1 H_2 : CO.

Electron microscopy was performed on a JEM-4000EX (resolution 1.7 Å) electron microscope at Arizona State University and a JEM-2000FX electron microscope at New Mexico (point resolution 3.0 Å). The catalyst powders were supported on holey carbons films on Cu grids. No solvents were used at any stage of the sample preparation; the grids were simply dipped into the powders and the excess powder was shaken off. We have shown previously that this method helps to minimize sample contamination in the microscopic (*20*). All catalyst samples were treated in the chemisorption system before examination in the electron microscope.

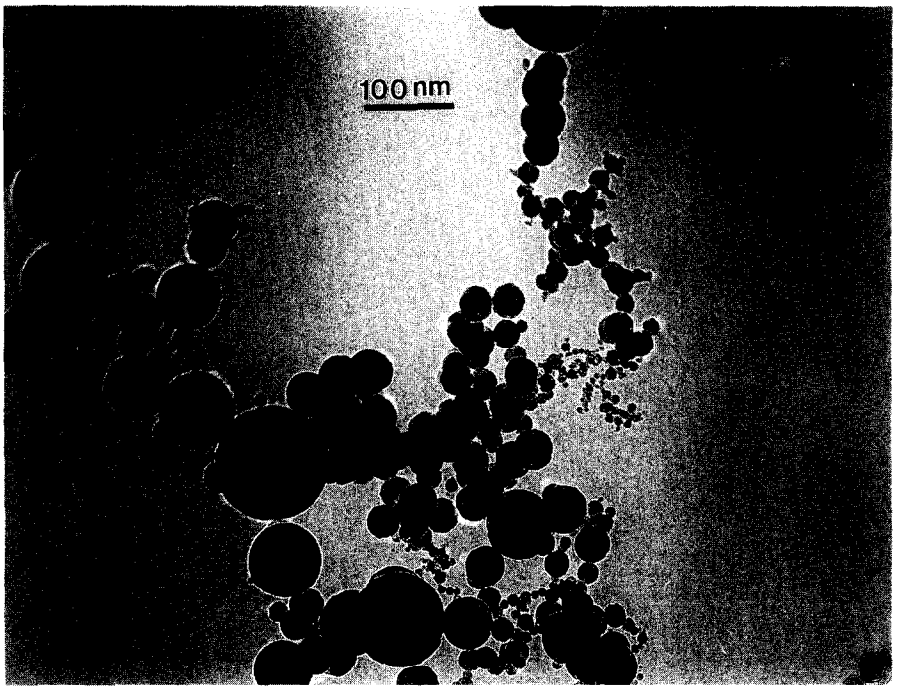

FIG. 1. Low-magnification micrograph of titania powder used in this study. The spherical particles are single crystals of the anatase or rutile phase.

RESULTS

Hydrogen Chemisorption

The chemisorption uptake of H_2 as a function of pretreatment is shown in Table 1. In all experiments, the reduction was performed overnight, approximately 16 h, and at a pressure of 200 Torr. The initial hydrogen uptake of the catalyst corresponds to a dispersion of 18% based on metal loading. The weight loading was approximately 2 wt% based on the amount of metal used during impregnation. The surface-average diameter of the Rh particles based on chemisorption was 5.3 nm which agrees with a TEM diameter of 5.0 nm. High-temperature reduction at 773 K caused a sharp drop in H_2 uptake. Table 1 shows that H_2 uptake was only partially recovered after overnight treatment at 200 Torr O_2 at 473 K. Oxidation at 573 K was necessary to recover most of the H_2 uptake.

TABLE 1

Hydrogen Chemisorption Uptake as a Function of Pretreatment of Rh/TiO_2 Catalyst

Treatment	Uptake (μmol/g)
LTR	17.5
HTR	2.9
473 K O_2-LTR (2 h)	6.1
473 K O_2-LTR (overnight)	14.7
573 K O_2-LTR (overnight)	15.5
673 K O_2-LTR (overnight)	15.5
773 K O_2-LTR (overnight)	18.0

Transmission Electron Microscopy

A high-resolution micrograph of the Rh/TiO_2 after initial low-temperature reduction is shown in Fig. 2. The surface structure of the Rh metal is clearly resolved. Lattice fringes can be seen in both the metal and the oxide support. The Rh metal surface appears clean and free of any contamination even though the catalyst was exposed to air after removal from the reactor for ex-

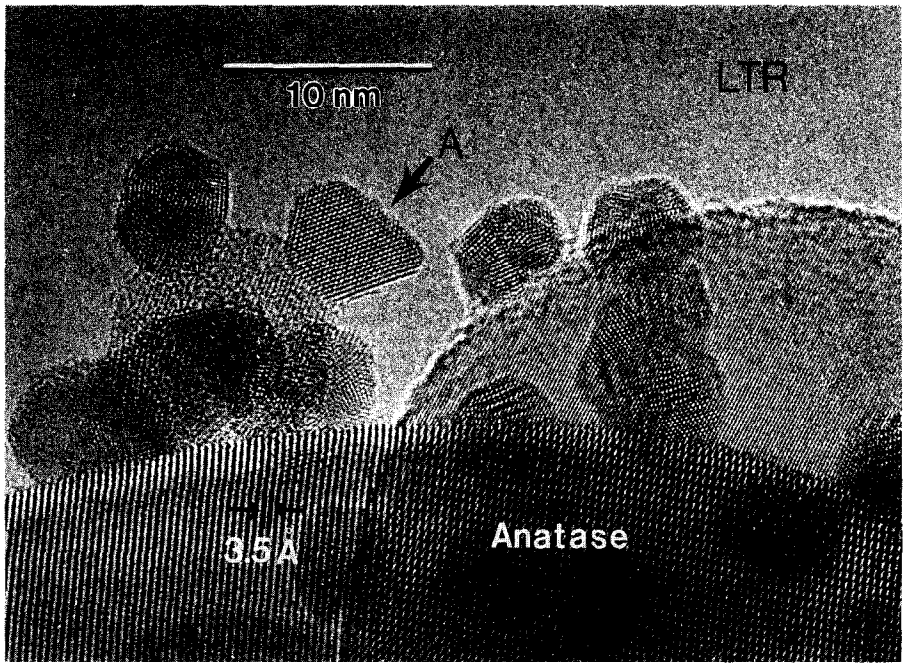

FIG. 2. High-resolution micrograph of Rh/TiO_2 after initial low-temperature reduction. The surfaces of the metal particles are clean, and most particles are multiply twinned.

amination in the TEM. Most of the Rh metal particles in this catalyst are multiply twinned as seen in Fig. 2. However, the particle labeled A is a single crystal whose lattice spacings do not correspond to bulk fcc Rh. Petford-Long *et al.* (*21*) have reported that small metal particles can exhibit several different crystal structures when exposed to the electron beam. For example, a Ru crystallite was observed to exist in the bcc, the fcc, and the hcp crystal structures in rapid succession (*21*). It has also been suggested recently that small particles may exhibit different crystal structures because the energy minima associated with these structures are quite shallow (*22*). Thus, the single-crystal particle A in Fig. 2, whose structure differs from that of bulk Rh, may represent a metastable structure. The 3.5-Å lattice fringes in the lower part of the micrograph can be indexed to anatase (*101*) lattice planes. The TiO_2 support particle on the right exhibits 1.66-Å lattice fringes which could arise from the rutile (211) or the anatase (211) planes but it is not possible to differentiate between either of these possibilities from this one-dimensional set of lattice fringes.

A micrograph of the Rh/TiO_2 sample following high-temperature reduction in hydrogen (HTR, 773 K, overnight) is shown in Fig. 3. The metal crystal structure is again well resolved and the metal particle near the center of the micrograph has lattice fringes corresponding to fcc Rh with a well-defined (111) twin boundry across the center of the particle. The particle is oriented close to the [01$\bar{1}$] zone. An overlayer between 0.2 and 0.4 nm thick is observed covering both the metal and the support. The overlayer thickness is not uniform across the surface of the metal particle, being thickest on the (100) and (111) low-index surface facets and thinnest where the low-index facets meet. This observation differs from that of Vanselow and Mundschau (*23*) who found that TiO_2 overlayers preferentially covered the high-index facets on a Pt

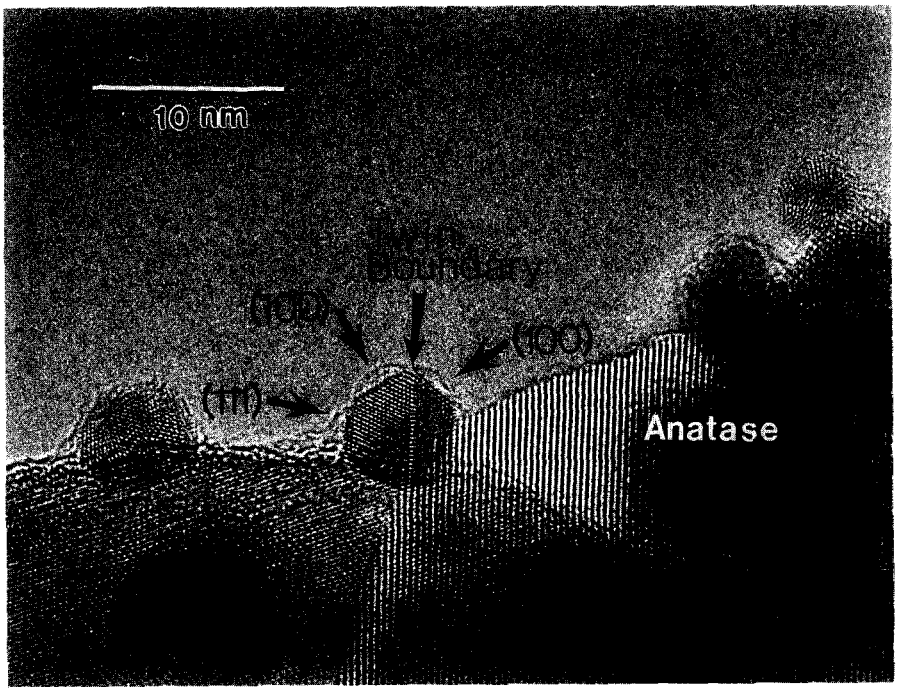

FIG. 3. Micrograph of the Rh/TiO_2 catalyst after-high temperature reduction. An amorphous overlayer is seen covering the metal as well as the support. This overlayer is most pronounced on the low-index facets of the metal.

field ion tip. In general, there are only a few particles that are oriented properly to allow the low-index facets to be clearly imaged. Therefore, it is not possible to generalize from the observation in Fig. 3. However, it is evident from all the micrographs we have obtained that the overlayer thickness is nonuniform. The support is still crystalline titania with lattice fringes that correspond to the anatase or rutile phases. There is no evidence in this or other micrographs for the presence of other crystalline phases of titania, such as Ti_4O_7.

The Rh/TiO_2 catalyst sample, after high-temperature reduction, was oxidized at 573 K overnight at 200 Torr of O_2 and examined in the microscope (Fig. 4). The metal crystallite surfaces appear rough so that the detection of amorphous overlayers is more difficult. An overlayer may still be present on the particles, but is not as pronounced as in Fig. 3. The overlayers on the oxide surface also appear considerably diminished after this treatment. The H_2 chemisorption uptake is almost completely restored on this catalyst.

Butane Hydrogenolysis

The activity and selectivity of these catalysts for the hydrogenolysis of *n*-butane as a function of pretreatment is shown in Figs. 5 and 6. Since H_2 chemisorption could not be performed *in situ* after each of the pretreatments in the flow reactor, we have chosen to base the turnover frequency on the initial H_2 uptake. However, we have also reported the reactivity based on independent hydrogen uptake measurements in the chemisorption system after similar pretreatments. The results show that the onset of the SMSI state is accompanied by a drop in hydrogenolysis activity of approximately three orders of magnitude. If the activity is normalized to the suppressed H_2 uptake after SMSI, the activity variation is approximately two orders of magnitude. The drop

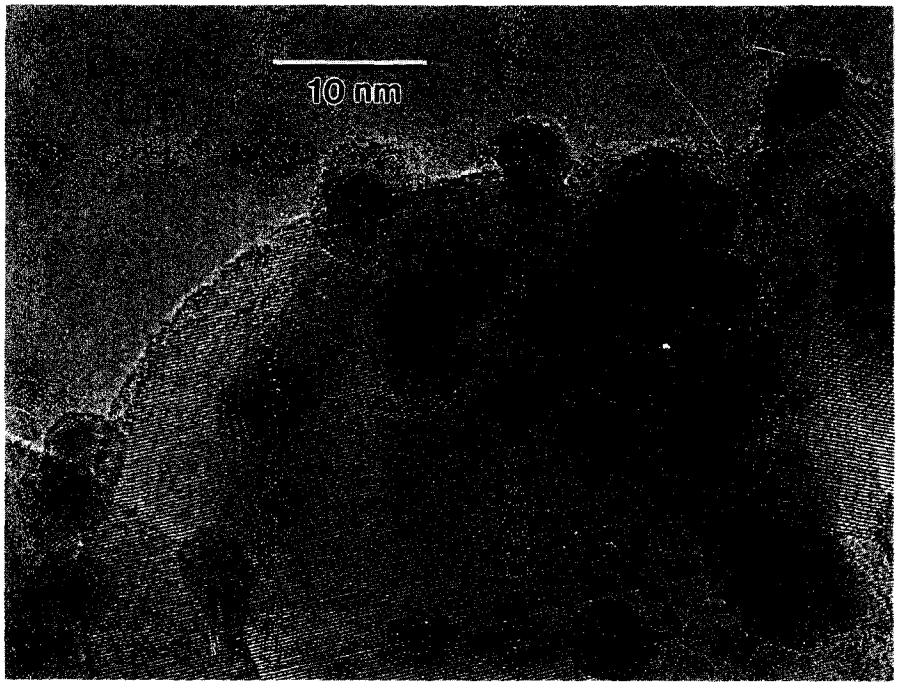

FIG. 4. Micrograph of the Rh/TiO_2 catalyst after HTR and oxidation at 573 K, followed by LTR.

in activity is also accompanied by an increase in percentage C_2 in the products, suggesting a greater tendency toward central bond scission in the SMSI state. The selectivity variations seen in Fig. 6 are similar to those seen on Rh/SiO_2 (*17, 24*) after comparable pretreatments. The activities and selectivities of the catalyst in the SMSI state were measured at 523 K since conversions were too low to measure at the reaction temperature used for the other runs (473 K). The data reported here for the SMSI state were extrapolated using an Arrhenius plot.

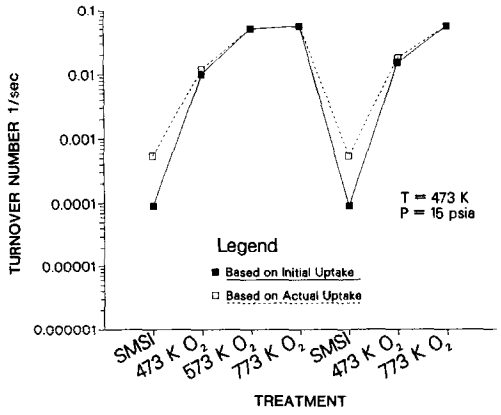

FIG. 5. *n*-Butane hydrogenolysis activity of catalyst Rh/TiO_2 as a function of treatment, measured at 473 K and 103.2 kPa. A three-order-of-magnitude drop in activity is observed under SMSI conditions.

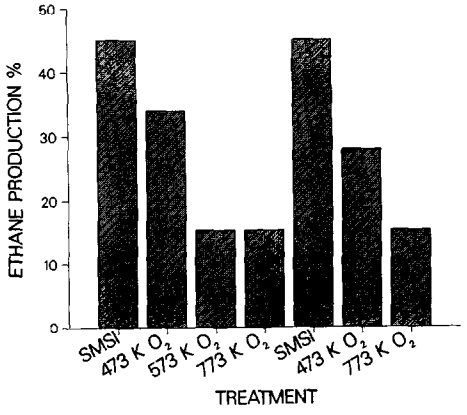

FIG. 6. Percentage ethane in the products of *n*-butane hydrogenolysis as a function of catalyst pretreatment. A product selectivity change of approximately 30% accompanies the drop in hydrogenolysis activity.

Figure 7 shows the *n*-butane hydrogenolysis activity of a 5% Rh/SiO_2 catalyst and a physical mixture of the Rh/SiO_2 and Rh/TiO_2 catalysts. The high-temperature reduction causes a drop in catalyst activity of about one order of magnitude. Oxidation followed by LTR restores the catalyst activity. The physical mixture exhibits activities that can simply be ascribed to an arithmetic mean of the activity of the SiO_2- and TiO_2-supported catalysts after the corresponding treatments. The product distribution on the physical mixture is similar to that on the Rh/SiO_2 catalyst.

CO Hydrogenation

The activity of Rh/TiO_2 for the CO hydrogenation reaction is reported in Fig. 8. The activity is reported as a turnover frequency based on the H_2 chemisorption uptake on the fresh catalyst. Figure 8 shows that the activity of the catalyst increases by a factor of 3 after HTR. Subsequent oxidation does not change the activity significantly and a second HTR actually causes a drop in activity. We have found that the behavior of the catalyst also depends on the precursor used during catalyst preparation. When a catalyst prepared using $Rh(Cl)_3 \cdot 3H_2O$ was examined, there was no increase in activity after HTR unlike that on the $Rh(acac)_3$-prepared catalyst seen in Fig. 8.

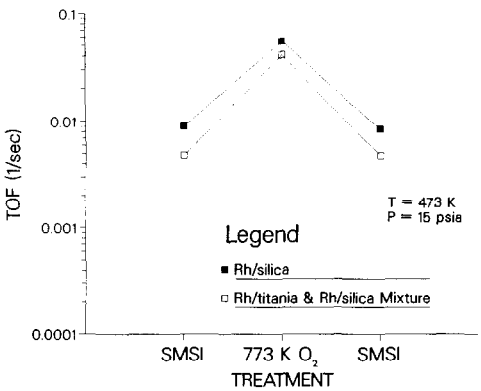

FIG. 7. *n*-Butane hydrogenolysis activity of a Rh/SiO_2 catalyst and a mixture of Rh/TiO_2 and Rh/SiO_2 at 473 K and 103.2 kPa.

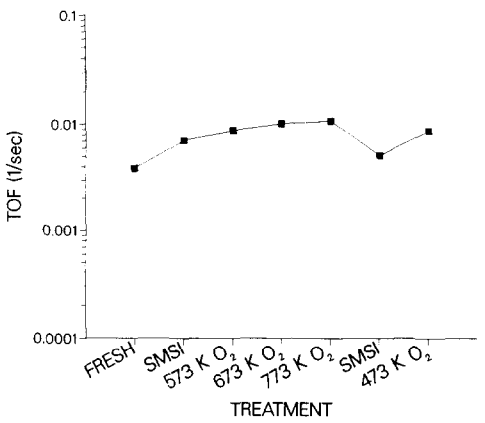

FIG. 8. CO hydrogenation activity of catalyst Rh/TiO_2 measured at 523 K and 103.2 kPa.

DISCUSSION

The model catalyst used in this study exhibits catalytic activity and chemisorption behavior that are comparable to those of Rh/TiO_2 catalysts reported in the literature (*7, 14, 25*). High-temperature reduction leads to a loss of H_2 chemisorption uptake that is recovered upon oxidation at 573 K followed by LTR. The high-resolution transmission electron microscopy images presented here show that the onset of SMSI is related to a buildup on the metal surface of 2 to 4-Å overlayers which are partially removed by subsequent oxidation and LTR. Only the amorphous nature and thickness of the overlayers can be observed; no other chemical information is available from the micrographs. On the basis of spectroscopic work in the literature (*26*), the overlayers are believed to be a suboxide of titania. Singh *et al.* (*27*) have previously reported observation of a similar overlayer on Rh crystallites subjected to HTR; however, micrographs of the fresh catalyst were not shown to firmly establish that the overlayer was indeed caused by HTR. Amorphous overlayers due to carbon contamination were unbiquitous in older generations of microscopes that were diffusion pumped. Newer microscopes (such as the JEOL 4000 EX used in this study) use ion pumps that minimize residual hydrocar-

bons in the specimen chamber. In this work great care has been taken to ensure that the overlayers did not arise due to spurious carbon contamination in the microscope. We have recently reported observations of the same area of the catalyst (at a lower resolution) after various pretreatments that confirm the presence of the overlayers after HTR (*28*).

The migration of the TiO_x onto the Rh metal surface and its subsequent removal are strikingly evident in all these micrographs. Figure 4 shows that the amount of amorphous overlayer is significantly reduced after oxidation. Since the Rh surfaces in Fig. 4 do not exhibit any pronounced surface facets, the amorphous overlayers are more difficult to detect. We attribute the absence of surface facets to roughening by high-temperature treatments in oxygen. Rh metal is easy to oxidize and by 573 K, 5 to 10-nm particles on SiO_2 have an oxide layer which is approximately 1 nm thick (*29*). The 90% volume increase upon oxidation of Rh and the lower mobility of the metal may leave behind a roughened surface. The electron micrographs do not provide conclusive evidence for restoration of surface structure after SMSI. Therefore, the reactivity of the Rh surfaces is a better indicator of the extent of reversal of the SMSI state.

The activity and selectivity of the Rh/TiO_2 are completely restored after oxidation at 573 K followed by LTR (Figs. 5 and 6). The data in these figures correspond to the catalyst after several treatment cycles. The activity of the fresh catalyst is not shown in this figure and was only marginally greater than the activity seen in the O_2-LTR state. Some sintering does occur during the first exposure of the catalyst to high temperatures, but the small particles are stable thereafter. The product distribution changes from about 10–15% C_2 after O_2-LTR to approximately 50% C_2 after SMSI. Bond *et al.* (*30*) observed a similar change in selectivity on Ru supported on TiO_2 after high-temperature reduction. The selectivity differences we observed were quite reproducible and the catalyst could be cycled repeatedly between the HTR and O_2-LTR states. Since the reactivity of the physical mixture of Rh/SiO_2 and Rh/TiO_2 resembles that of Rh/SiO_2, we conclude there is no transport of the TiO_x onto the SiO_2 spheres.

The variation in hydrogenolysis activity after HTR and O_2-LTR should be understood in the light of results on SiO_2-supported Rh (*17, 24*) where strong metal–support interactions are not expected to occur. Figure 7 shows that butane hydrogenolysis activity on Rh/SiO_2 drops by approximately one order of magnitude after reduction at 773 K and the activity is restored by oxidation followed by LTR. On Rh/TiO_2, when the turnover frequency for *n*-butane hydrogenolysis is based on the actual H_2 chemisorption uptake (dotted curve in Fig. 5), the activity variations between the HTR and the O_2-LTR state are approximately two orders of magnitude. Thus, high-temperature reduction leads to a drop in activity in both cases. The selectivity variations on the SiO_2- and TiO_2-supported catalysts are also very similar and the percentage C_2 in the products increases after HTR to 50% and drops to 10–20% after O_2-LTR. The activity and selectivity variations in the Rh/SiO_2 catalyst are caused by the surface structure variations induced by O_2–H_2 cycling (*17*). Variations in catalyst activity caused by surface oxidation have also been reported previously by other researchers. For instance, Burwell (*31*) observed a drop in methylcyclopropane hydrogenolysis activity on Pd/SiO_2 when the reduction temperature was increased from 373 to 723 K. The catalyst had been subjected to a standard pretreatment involving exposure to O_2 to 573 K and hence one would expect the surface to be in an oxidized state. A more drastic oxidation step (803 K) was used by Taylor *et al.* (*32*) for supported Ru. They observed that the "high" activity state seen after oxidation was lost after hydrogen reduction at 923 K. Hence, it is quite plausible that the activity changes seen on the

TiO_2-supported Rh are also caused, in part, by surface structure variations induced by O_2–H_2 cycling.

In addition to the surface structure variation, the high-temperature reduction of Rh/TiO_2 leads to coverage of the Rh by amorphous overlayers. The chemisorption uptake of H_2 dropped from 17.5 to 2.9 μmole/g suggesting that only 17% of the surface Rh atoms may be exposed to the gas phase while the rest are covered by the amorphous overlayers. The electron micrographs in this study (Fig. 3) imply surface coverage of the Rh far greater than the 83% or so suggested by the chemisorption uptake. Since there is evidence for spillover of H_2 over the support in the SMSI state (*33*), the measured H_2 uptake in the SMSI state includes some of the H_2 which may sit on the support. This makes it difficult to quantify the extent of coverage of the Rh by the TiO_x overlayers using chemisorption. The electron micrographs also show that overlayer thickness is not uniform on a given particle and varies in thickness over the Rh particles examined. Since the hydrogenolysis reaction proceeds faster on small particles (*34*) and on highly dispersed Rh (*35*), it would be incorrect to ascribe the activity variations induced in the SMSI state to ensemble effects. Thus, it is likely that the hydrogenolysis activity measured in the SMSI state is the activity due to the small number of Rh atoms still accessible to gas-phase reactants. This is consistent with the results of Williams *et al.* (*36*) who observed a linear decrease in ethane hydrogenolysis activity with increasing titania coverage.

The influence of high-temperature reduction and subsequent oxidation on the CO hydrogenation reaction is different from that in butane hydrogenolysis. On Rh/SiO_2, we have found that the turnover frequency for methanation does not change significantly after these pretreatments. Figure 8 shows that the activity of the Rh/TiO_2 catalyst increases after the first HTR and does not vary markedly with subsequent oxidation treatments. A second HTR causes the activity to go down slightly. We found that these trends were not very reproducible, and the activity sometimes increased a little or on other occasions decreased after the oxidation. Previous work by Demmin *et al.* (*37*) and by Levin *et al.* (*38*) has demonstrated that the activity in CO hydrogenation can increase upon exposure of polycrystalline Pt or Rh foils to TiO_2. Levin *et al.* (*38*) showed there is an optimal coverage for maximum reactivity, suggesting thereby that the sites of higher activity were the Rh atoms in proximity to the TiO_x, i.e., on the island perimeters. The calibration by Williams *et al.* (*39*) shows the optimal coverage to be $\theta = 0.45$–0.50. Our results are in agreement with this model. Since the fresh catalyst starts off with a clean Rh surface, the activity goes up after the first HTR. Subsequent oxidation causes partial reversal of the SMSI by removal of the overlayers. The activity after the oxidation can go up or down depending on the coverage of TiO_x achieved after the HTR. Subsequent prolonged reduction can cause a decrease in activity due to excessive surface coverage by the TiO_x.

A significant feature of this study is that the $Rh(acac)_3$ precursor used during catalyst preparation did not cause any solubilization of the TiO_2 during impregnation. We have found that use of acidic precursors can cause extensive dissolution of the oxide which leads to the presence of amorphous surface layers on the TiO_2 surface. On high-surface-area catalysts, such phenomena often go unnoticed since the morphology of the initial oxide power is not well defined. In a previous study, we found that MgO was completely transformed to $Mg(OH)_2$ during impregnation with $RuCl_3 \cdot 3H_2O$ (*40*) at room temperature. The influence of oxide dissolution and redeposition becomes evident when the reactivity behavior of a catalyst prepared using the $RhCl_3 \cdot 3H_2O$ precursor is compared to a $Rh(acac)_3$-prepared catalyst. The activity of the $RhCl_3 \cdot 3H_2O$-prepared catalyst in CO hydrogenation did not increase after the first

high-temperature reduction. This suggests that the Rh surface was already covered with sufficient TiO_2 to help in the reaction. The enhanced activity seen on TiO_2-supported catalysts even before high-temperature reduction (*16*) is, we believe, due to use during catalyst preparation of acidic precursors which may deposit enough TiO_2 on the surface to assist in the CO hydrogenation reaction. Levin *et al.* (*38*) have shown that extensive prereduction of a TiO_2-promoted surface is not necessary to see an activity enhancement. In fact, reduction of the support and reoxidation may be occurring during the course of the catalytic cycle involving CO hydrogenation. The TiO_x overlayers are obviously being modified during the course of the reaction, which explains why the reaction proceeds on a surface that appears almost completely encapsulated as in Fig. 3. When we performed a butane hydrogenolysis after CO hydrogenation on Pt/TiO_2, we observed a partial restoration of hydrogenolysis activity suggesting that the number of Pt atoms exposed to the gas phase had increased.

CONCLUSIONS

High-resolution transmission electron microscopy is useful for imaging the surface structure and the presence of sub-nm overlayers on metal particles in heterogeneous catalysts. The correlation between reactivity and structure is facilitated by the ability to measure the reactivity and chemisorption of the same catalyst used for electron microscopy. The catalyst characterization by high-resolution TEM is consistent with the development of amorphous overlayers of TiO_x upon high-temperature reduction. These overlayers are removed by oxidation followed by low-temperature reduction. The Rh metal surface after this O_2-LTR treatment looks different from the initial Rh surface, suggesting that a surface roughening may occur due to the oxidation–reduction treatment.

A drop in activity is observed after high-temperature reduction on both TiO_2- and SiO_2-supported Rh. On SiO_2-supported Rh, the drop in activity is believed to be due to annealing of the O_2-roughened surface and is typically one order of magnitude under our experimental conditions. On TiO_2-supported Rh, the drop in activity is more pronounced (three orders of magnitude) and is due, in part, to site blocking by amorphous TiO_x overlayers. The selectivity changes after HTR are similar on both TiO_2- and SiO_2-supported catalysts. In both cases, the percentage C_2 in the products goes up after HTR and drops after O_2-LTR. A particle size effect is not directly responsible for these variations since no particle size change occurs after HTR or after O_2-LTR.

The variation in the CO hydrogenation activity is consistent with a TiO_x-assisted pathway for CO dissociation. On small Rh metal crystallites 50 Å in diameter, the number of interfacial sites is limited. High-temperature reduction causes migration of TiO_x overlayers leading to enhanced activity. The activities in CO hydrogenation are somewhat irreproducible since they depend on the exact sequence of steps, i.e., reduction temperature, pressure, and duration. Prolonged reduction leading to near-monolayer coverage causes a drop in activity. However, the activity variations are no more than a factor of 3. We believe that the CO hydrogenation reaction leads to restructing of these overlayers and an increase in the number of Rh atoms exposed to the surface. These overlayers also lead to an increase in the amount of C_2^+ hydrocarbons in the products of CO hydrogenation, in agreement with previous workers.

ACKNOWLEDGMENTS

Financial support for this work from the NSF (Grant CBT-8707693) is gratefully acknowledged. Electron microscopy was performed at the Electron Microbeam Analysis Facility, Department of Geology, University of New Mexico, and at the NSF National Facility for High Resolution Electron Microscopy within the Center for Solid State Science, Arizona State University (supported by Grant DMR-86-11609).

REFERENCES

1. Tauster, S. J., Fung, S. C., and Garten, R. L., *J. Amer. Chem. Soc.* **100,** 170 (1978).
2. Vannice, M. A., and Garten, R. L., *J. Catal.* **56,** 236 (1979).
3. Vannice, M. A., and Sen, B., *J. Catal.* **113,** 52 (1988).
4. Ko, E. I., and Garten, R. L., *J. Catal.* **68,** 233 (1981).
5. Foger, K., *J. Catal.* **78,** 406 (1982).
6. Belton, D. N., Sun, Y. M., White, J. M., *J. Amer. Chem. Soc.* **106,** 3059 (1984).
7. Resasco, D. E., and Haller, G. L., *J. Catal.* **82,** 279 (1983).
8. Santos, J., Phillips, J., and Dumesic, J. A., *J. Catal.* **81,** 147 (1983).
9. Cunningham, J., and Al-Sayyed, G. H., *Surf. Sci.* **169,** 289 (1986).
10. Baker, R. T. K., Prestidge, E. B., and Garten, R. L., *J. Catal.* **59,** 292 (1979).
11. Rieck, J. S., and Bell, A. T., *J. Catal.* **99,** 262 (1986).
12. Vannice, M. A., and Twu, C. C., *J. Catal.* **82,** 213 (1983).
13. Kikuchi, E., Matsumoto, M., Takahashi, T., Machino, A., and Morita, Y., *Appl. Catal.* **10,** 251 (1984).
14. Meriaudeau, P., Ellestad, O. H., Dufaux, M., and Naccache, C., *J. Catal.* **75,** 243 (1982).
15. Ko, E. I., Hupp, J. M., and Wagner, N. J., *J. Catal.* **86,** 315 (1984).
16. Bracey, J. D., and Burch, R., *J. Catal.* **86,** 384 (1984).
17. Braunschweig, E. J., Logan, A. D., Chakraborti, S., and Datye, A. K., *in* "Proceedings, 9th International Congress on Catalysis, Calgary, 1988" (M. J. Phillips and M. Ternan, Eds.), p. 1122. Chem. Institute of Canada, Ottawa.
18. Uyeda, R., *J. Crystal Growth* **24/25,** 69 (1974).
19. Iijima, S., *Jap. J. Appl. Phys. L* **347,** 23 (1984).
20. Logan, A. D., Braunschweig, E. J., Datye, A. K., and Smith, D. J., *Langmuir* **4,** 827 (1988).
21. Petford-Long, A. K., Long, N. J., Smith, D. J., Wallenberg, L. R., and Bovin, J. O., *in* "Physics and Chemistry of Small Clusters" (P. Jena, B. K. Rao, and S. N. Khanna, Eds.), p. 127. Plenum, New York, 1987.
22. Ajayan, P. M., and Marks, L. D., *in* "Mat. Res. Soc. Symp. Proc." (M. M. J. Treacy *et al.*, Eds.), Vol. 111, p. 53, 1988.
23. Vanselow, R., and Mundschau, M., *J. Catal.* **103,** 426 (1987).
24. Gao, S., and Schmidt, L. D., *J. Catal.* **111,** 210 (1988).
25. Resasco, D. E., and Haller, G. L., *J. Phys. Chem.* **86,** 4552 (1984).
26. Sadeghi, H. R., and Henrich, V. E., *J. Catal.* **81,** 279, (1984).
27. Singh, A. K., Pande, N. K., and Bell, A. T., *J. Catal.* **94,** 422 (1986).
28. Braunschweig, E. J., Logan, A. D., and Datye, A. K., *in* "Mat. Res. Soc. Symp. Proc." (M. M. J. Treacy *et al.*, Eds.), Vol. 111, p. 35, 1988.
29. Logan, A. D., Braunschweig, E. J., Datye, A. K., and Smith, D. J., *Ultramicroscopy*, in press.
30. Bond, G. C., Rajaram, R. R., and Burch, R., *in* "Proceedings, 9th International Congress on Catalysis, Calgary, 1988" (M. J. Phillips and M. Ternan, Eds.), p. 1130. Chem. Institute of Canada, Ottawa.
31. Burwell, R. L., *Langmuir* **2,** 2 (1986).
32. Taylor, K. C., Sinkevitch, R. M., and Klimisch, R. L., *J. Catal.* **35,** 34 (1974).
33. Jiang, X-Z., Hayden, T. F., and Dumesic, J. A., *J. Catal.* **83,** 168 (1983).
34. Yates, D. J. C., and Sinfelt, J. H., *J. Catal.* **8,** 348 (1967).
35. Yao, H. C., Yu Yao, Y.-F., and Otto, K., *J. Catal.* **56,** 21 (1979).
36. Williams, K. J., Levin, M. E., Bell, A. T., and Somorjai, G. A., *Catal. Lett.* **1,** 331 (1988).
37. Demmin, R. A., Ko, C. S., and Gorte, R. J., *J. Phys. Chem.* **89,** 115 (1985).
38. Levin, M. E., Salmeron, M., Bell, A. T., and Somorjai, G. A., *J. Catal.* **106,** 401 (1987).
39. Williams, K. J., Salmeron, M., Bell, A. T., and Somorjai, G. A., *Surf. Sci.* **204,** L745 (1988).
40. Holt, T. E., Logan, A. D., Chakraborti, S., and Datye, A. K., *Appl. Catal.* **34,** 199 (1987).